Cross Correlate Tidal Reconstructed 21cm Signal with Kinematic Sunyaev-Zel'dovich Effect: A New Probe for Missing Baryons at $z \sim 1-2$

The kinetic Sunyaev-Zel'dovich(kSZ) effect on Cosmic Microwave Background(CMB), induced by radial momentum of hot electrons, is a powerful source to probe baryon distributions. However, the signal is weak and lack of redshift information, hence another survey with spectroscopic redshift is typically required. This largely limits the sky area and depth to harness kSZ. Here, we propose a new source for cross correlation— HI density field from 21cm intensity mapping. 21cm spectra provide accurate redshift and intensity mappings integrate weak diffuse spectra, and thus can survey large sky area with great depth in much shorter time with low costs.

One main concern of the method is that the complicate 21cm foregrounds will contaminate radial large scale information, and reduce the correlation with kSZ. For redshift 1 and 2, we imitate the foreground substraction in simulations, and find that after velocity reconstructions, there is $\gtrsim 0.5$ correlation with kSZ signal for $l \gtrsim 1000$, and it drops fast for $l < 1000$. To improve the behavior, we recover large scale modes from their tidal influence on small scale structures (Cosmic Tidal Reconstruction). Successfully recover $> 90\%$ information at $k \sim 0.01h/Mpc$, we obtain a new $r > 0.6$ correlation for $l \sim 100 - 2000$, which corresponds to $S/N > 3$ for $l \sim 500 - 3000$ with Planck noise. Since the reconstructed field and foreground substracted field are superior in different modes, it is easy to combine them and get better S/N

PACS numbers:

I. INTRODUCTION

While the baryon abundance of early universe is well fixed [1][2][3][4], at $z \lesssim 2$ the detected baryon content in collapsed objects, eg. galaxies, galaxy clusters and groups, only account for 10% of the predicted amount. More baryons are believe to reside in Warm-Hot Intergalactic Mediums (WHIM) with typical temperature of 10^5 K to 10^7 K [5][6], which is too cold and diffuse to be detected. Continuous effort has been made to detect this part of baryons. One common approach is using hydrogen and metal absorption lines(eg, HI, Mg II,Si II, C II, Si III, C III, Si IV, O VI, O VII) [7][8]. However, the lines are usually limited to close circumgalactic medium, while at least 25% of the baryons are bebieved to reside in more diffused region [9]. Moreover, the uncertainty in metalicity would sometimes reduce the reliability.

A promising tool to probe the missing baryon is the kinetic Sunyaev-Zel'dovich(kSZ) effect [10][11], an effect that is greatly known for its potential to explore the Epoch of Reionization [12][13][14]. It refers to the secondary temperature anisotropy in CMB caused by Compton-scattering with free electrons. Since kSZ signal only relates to electron density and radial velocity, regardless the temperature and pressure, and velocity mainly results from large scale structure, the method is less biased towards hot, compact place, and provide more information on the fraction of diffused baryons.

Attractive as it is, due to the contamination of primary CMB, facility noises and probably residual thermal SZ signal, it is difficult to filter for the kSZ signal independently. Worse still, the signal itself does not contain redshift information.

To fix this, previous approches cross correlated it with galaxy surveys, eg. using pairwise-momentum estimator [15] or velocity-field-reconstruction estimator [16][17]. However since they all require spectroscopy of galaxies to provide accurate redshift, the sky volume and redshift range to apply the method is limited. A recent effort try to fix this using projected fields of galaxies, which is cheap and feasible [18]. However, projected fields only use information of $k_z = 0$ modes of galaxy overdensity, while for $l \gtrsim 1000$, where primary CMB fades away, a sufficient amount of kSZ signal is from non-zero k_z. This limits the accuracy and S/N it can reach.

In this paper we put forward a new source for cross correlation—HI density field from 21cm intensity mapping. Density contrast from 21cm spectra have accurate redshift information, which enables us to reconstruct velocity field and get better correlation with kSZ powerspectra. Moreover, intensity mapping is a kind of surveys that integrates different signals, rather than distinguishing individual galaxies. It accumulates contributions from weak sources and hence be able to reach high S/N at shorter time. There are already several ongoing 21cm experiments aim at large sky coverage and claim to be able to reach $z \gtrsim 1$ in very near future. CHIME [19], Tianlai [20], HIRAX [21] etc. Therefore, this correlator is more feasible than large galaxy spectroscopic surveys, and more accurate that projected field.

However, the 21cm density field has its own drawback—the complicated foregrounds results from integration. While a cosmic signal in 21cm measurement is of the order of mK, foregrounds coming from Galactic emissions, telescope noise, extragalactic radio sources and Radio recombination lines, can reach the order of Kelvin [22][23]. Lots of techniques have been developed to substract the foregrounds, taking advantage of the attribute that they have fewer bright spectral degrees of freedom[24]. Unfortunately, substraction will contaminates the smooth large scale structure information in radial direction. Since the kSZ signal coming from a both density and velocity field, and velocity is greatly related to large scale structures. This drawback will inhibit the cross correlation behavior.

In this paper, we first discuss the influence of foregrounds and small scale noises, based on simulation and analysis. To improve the correlation, we for the first time apply a 3D version of a new method called Cosmic Tidal Reconstruction [25][26], which recover the large scale modes of density field from its tidal influence on small scale structures.

The paper is organized as follows: In section II, we demonstrate given a density field, how to correlate with kSZ signal with velocity reconstruction; In section III, we present the

result of cross correlation with foreground substracted field and discuss the behavior; Then in section IV, we introduce the method of 3D tidal reconstruction, and present the correlation results after small k modes recovered, In section V, we estimate statistical errors, discuss redshift distortion and possible improvements; and we conclude at section VI.

Notes: Throughout the paper, We use the $z = 1, 2$ output of six N-body simulations from the CUBEP^{3}M code [27], each evolving 1024^3 particles in a $(1.2\mathrm{Gpc}/h)^3$ box. Simulation parameters are as follows: Hubble parameter $h = 0.678$, baryon density $\Omega_b = 0.049$, dark matter density $\Omega_c = 0.259$, amplitude of primordial curvature power spectrum $A_s = 2.139 \times 10^{-9}$ at $k_0 = 0.05\ \mathrm{Mpc}^{-1}$ and scalar spectral index $n_s = 0.968$.

we use "$\wedge$" to denote recontructed fields as oppose to fields directly from simulations.

II. VELOCITY RECONSTRUCTION AND KSZ SIGNALS CROSS CORRELATION

Given a density field, due to the cancellation of positive and negative velocity, its direct cross correlation between kSZ signal will vanish. Here, we apply a method that first calculates the linear peculiar velocity from density field, and then generate a mock kSZ signal following the same equation as the real signals. [16]. In this way, we can at most maximize the correlation.

Assume we have a density contrast field $\delta = \frac{\rho - \bar{\rho}}{\bar{\rho}}$, where $\bar{\rho}$ is the average density of a certain redshift slice.

Basic steps to get the cross correlation are as follows.

(1) Estimate the velocity field:

In linear region, the continuity equation goes like: $\dot{\delta} + \nabla \cdot \boldsymbol{v} = 0$, where $\boldsymbol{v}$ is the peculiar velocity and δ is the matter overdensity.

Therefore, we obtain an estimator of velocity distribution from the density contract δ:

$$\hat{v}_z(\boldsymbol{k}) = iaHf\delta(\boldsymbol{k})\frac{k_z}{k^2} \tag{1}$$

where $f = \frac{d\ln D}{d\ln a}$, D(a) is the linear growth function, a is the scale factor, H is the Hubble parameter.

$v_z \propto \frac{k_z}{k^2}$, indicating the most prominent signal comes from small k mode, which corresponds to large scale structure. This further verify our motivation for tidal reconstruction procedure.

(2) suppress the noise in velocity field with a Wiener filter. This is because the term $\frac{k_z}{k^2}$ in Eq.(1) will strongly amplify noises in small k modes.

$$\hat{v}_z^c(\boldsymbol{k}) = \frac{\hat{v}_z(\boldsymbol{k})}{b(k_\perp, k_\parallel)} W(k_\perp, k_\parallel)\ , \tag{2}$$

Bias $b = \frac{P_{\hat{v}_z, v_z}}{P_{v_z}}$, Wiener filter $W = \frac{P_{v_z}}{P_{\hat{v}_z}/b^2}$.

(3) Calculate 2D kSZ map.

The CMB temperature fluctuations caused by kSZ effect is:

$$\Theta_{kSZ}(\hat{n}) \equiv \frac{\Delta T_{kSZ}}{T_{\mathrm{CMB}}} = -\frac{1}{c}\int d\eta g(\eta)\boldsymbol{p}_\parallel\ , \tag{3}$$

where $\eta(z)$ is the comoving distance at redshift z, $g(\eta) = e^{-\tau} d\tau/d\eta$ is the visibility function, τ is the optical depth to Thomson scattering, $\boldsymbol{p}_\parallel = (1+\delta)\boldsymbol{v}_\parallel$, with δ the electron overdensity. We assume that $g(\eta)$ doesn't change significally in one redshift bin, and integrate $\boldsymbol{p}_\parallel$ along radial axis to get $\hat{\Theta}_{kSZ}$

(4) Calculate correlation coefficients.

We compare reconstructed kSZ signals $\hat{\Theta}_{kSZ}$ with kSZ signals Θ_{kSZ} directly from simulations. To quantify the tightness of correlation, we employ a quantity r:

$$r \equiv \frac{P_{recon,real}}{\sqrt{P_{recon}P_{real}}} \tag{4}$$

III. CROSS CORRELATION WITH NOISE SUBSTRACTED FIELD

A. Mimic the Noise Substraction

To ressemble realistic observations, we take into account the resolution, small scale noises and foreground substractions. We apply two filters on original density contrast δ to imitate the effects of noise substractions:

1. Import a cut off scale k_c, with a step function $J(k_c - k)$ with $J(x) = 0, x < 0; J(x) = 1, x \geqslant 0$. This is reasonable for a filled aperture experiment, which has good brightness sensitivity and an exponetially growing noise at small scales. We choose $k_c = 0.5\ h/\mathrm{Mpc}$ and $0.32h/\mathrm{Mpc}$ respectively for $z = 1$ and $z = 2$, which corresponds to $\ell \sim 1150$. This is generally realistic, judging from ongoing 21cm experiments like CHIME [19][28] and Tianlai [29][20].

2. Use a high pass filter $W_{fs}(k_\parallel) = 1 - e^{-k_\parallel^2 R_\parallel^2/2}$ to imitate the foreground substraction. We choose $R_\parallel = 15\ \mathrm{Mpc}/h$ for $z = 1$ and $R_\parallel = 8\ \mathrm{Mpc}/h$ for $z = 2$, which gives $W_{fs} = 0.5$ at $k_\parallel = 0.08\ \mathrm{Mpc}/h$ and $0.15\ \mathrm{Mpc}/h$ respectively.

The observed 21cm field after foreground subtraction is then given by

$$\delta_{fs}(\boldsymbol{k}) = \delta(\boldsymbol{k}) W_{fs}(k_\parallel) J(k_c - k), \tag{5}$$

where $\delta(\boldsymbol{k})$ is the original density field from simulation,

With the noise substracted density contrast δ_{fs}, we follow the procedure described in last section to generate a mock kSZ signal $\hat{\Theta}_{fs}$ and calculate cross correlation $r_{\Theta,\hat{\Theta}_{fs}}$.

B. Cross Correlation Behavior with Noise Substracted Field

Fig.1 upper panel Shows the cross correlation between the reconstructed velocity field $\hat{v}_{z,ns}$ and the real velocity field v_z, at redshift 1 and 2.

At this point, all the manipulation and calculation on $\delta(\boldsymbol{k})$ are independent over different $\boldsymbol{k}$, therefore, the cross-correlation closely resembles the substraction we perform.

Just one interesting thing to notice is that although the foreground at z=2 is stronger, the non-linear effects are weaker. So

we still can obtain correlations at $k \lesssim 0.1$ from the seriously suppressed density contrast.

Fig.2 shows the cross correlation between the reconstructed kSZ map $\hat{\Theta}_{ns}$ and real kSZ map Θ at redshift 1 and 2. There are two points to notice:

(1) For both redshift, there are a considerable amount of correlation $r \gtrsim 0.5$ for $l \gtrsim 1000$; and this correlation drops quickly for smalller l;

(2) The obtained correlation at redshift 2 is better than redshift 1.

To explain the behavior of the cross correlation, we write Eq.(3) in Fourier space.

$$\begin{aligned}\Theta(\boldsymbol{k}'_\perp) \equiv\ \Theta\ (k'_x, k'_y, 0) &\propto \int d^3k\delta(\boldsymbol{k}'_\perp - \boldsymbol{k}_\perp, k_\parallel)v_z(\boldsymbol{k}) \\ \xrightarrow[region]{linear} &\int\ d^3k\delta(\boldsymbol{k}'_\perp - \boldsymbol{k}_\perp, k_\parallel)\delta(\boldsymbol{k})\frac{k_z}{k^2} \\ = &\int\ d^3lnk\delta(\boldsymbol{k}'_\perp - \boldsymbol{k}_\perp, k_\parallel)\delta(\boldsymbol{k})\frac{k_z^2 k_x k_y}{k^2}\end{aligned} \tag{6}$$

We transform $dk \to dlnk$ to show the contributions from different k scales. The strength of $|\delta(\boldsymbol{k})|$ with respect to k can be seen in Fig.**??**

For small $k'_\perp = l/\chi \sim 0.1$ h/Mpc:

Although $\frac{k_z^2 k_x k_y}{k^2}$ favors larger k, both $\delta(\boldsymbol{k}'_\perp - \boldsymbol{k}_\perp, k_\parallel)$ reach peak at $k \sim 0.1h/Mpc.$ and this makes a sufficient amount of contributions to the final integrated Θ. On the other hand, the fields after foreground substraction lack the part from small k_z, which caused the null correlation.

For large $k'_\perp \sim 1$h/Mpc:

$\delta(\boldsymbol{k}'_\perp - \boldsymbol{k}_\perp, k_\parallel)$ and $\delta(\boldsymbol{k})$ no longer reach peak at similar points. $\delta(\boldsymbol{k}'_\perp - \boldsymbol{k}_\perp, k_\parallel)\delta(\boldsymbol{k})$ has similar value for $k \sim 0.1$ h/Mpc and $k \sim 1$ h/Mpc, while $\frac{k_z^2 k_x k_y}{k^2}$ weights the later a hundred times heavier. Therefore, the importance of small k modes is attenuated.

Fig.**??** is a set of plots that helps understand the behavior.

The reason why the correlation on redshift 2 is better is that the density contrast at redshift 1 is sharper than redshift 2, which exaggerates the contribution from small scales.

Although performs badly at small l, the reconstructed kSZ signal $\hat{\Theta}_{ns}$ from 21cm density field shall still be able to give us reasonable S/N in real applications , because most kSZ signals that can be distinguished come from $l \gtrsim 1000$, when primary CMB gradually dies out.

However, based on the analysis above, we will expect a further improvement on cross correlation if we recover the small k modes lost in noises. In next section, we provide a method to achieve the goal.

IV. 3D COSMIC TIDAL RECONSTRUCTION

A. Algorithm

The cosmic tidal reconstruction is a kind of quadratic statistics developed to extract large scale information from alignment of small scale structures. It uses the second order density variance on small scales to solve for the large scale tidal shear and hence gravitational potential.

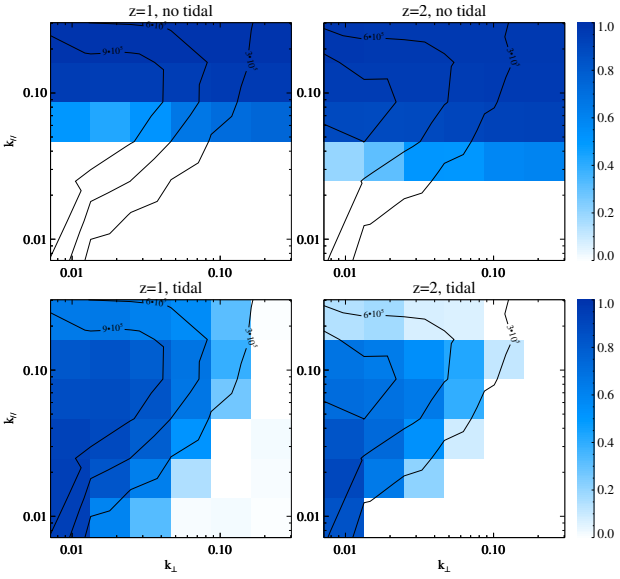

FIG. 1: (Top) The cross correlation r between P_{v_z} and $P_{\hat{v}_z^{fs}}$ calculated from foreground substracted field δ_{fs}; (Bottom) The cross correlation between P_{v_z} and $P_{\hat{v}_z^{tide}}$ calculated from $\hat{\kappa}_c$. The contour line indicates $k^3P(k)$.

Here, we present a complete 3 dimentional reconstruction algorithm that works best in close linear regions.

First, we smooth the density contrast to reduce the non-gaussianity. (1) Convolve the field with a Gaussian kernal $S(\boldsymbol{k}) = e^{-k^2R^2/2}$, we take $R = 1.25$ Mpc$/h$ [25], to reduce the complicated non-linear effects on small scales.

(2) Gaussianize the field, taking $\delta_g = \ln(1+\delta)$. This is to allieviate the problem that filter W_i in Eq.(10) heavily weights high density regions.

Second, we filter for the small scale structures that are most likely to be influenced by tidal force of large scale fields and calculate its variance. With it, we estimate the tidal force and reconstruct the large scale density field.

The local tidal distorted power spectrum is given by

$$P(\boldsymbol{k},\tau)|_{t_{ij}} = P_{1s}(k,\tau) + \hat{k}^i\hat{k}^j t_{ij}^{(0)} P_{1s}(k,\tau)f(k,\tau), \tag{7}$$

(1) Following gravitational lensing procedures, we decompose the 3×3 symmetric, traceless tidal force tensor, defined as

$$t_{i,j} = \Phi_{L,ij} - (1+\kappa_{3D})\delta^D_{ij}, \tag{8}$$

$\Phi_{L,ij}$ is the large scale potential, κ_{3D} is the large scale density contrast we want to get, δ^D is the Dirac function. into 5 γ components,

$$t_{ij} = \begin{pmatrix} \gamma_+ - \gamma_z & \gamma_\times & \gamma_x \\ \gamma_\times & -\gamma_+ - \gamma_z & \gamma_y \\ \gamma_x & \gamma_y & 2\gamma_z \end{pmatrix}. \tag{9}$$

(3) Apply filter $W_i(\boldsymbol{k})$, which assigns weights and calculate variance to δ_g according to predicted displacements caused by tidal field in near linear regions [26].

$$\delta_g^{w_i}(\boldsymbol{k}) = W_i(\boldsymbol{k})\delta_g(\boldsymbol{k}), \qquad (10)$$
$$W_i(\boldsymbol{k}) = i(\frac{P(k)f(k)}{P_{tot}^2(k)})^{\frac{1}{2}}\frac{k_i}{k} = S(k)\frac{k_i}{k}$$

i indicates $\hat{x}, \hat{y}, \hat{z}$ directions, $P_{tot} = P + P_{noise}$ is observed matter powerspectrum, P is theoretical matter powerspectrum, $f = 2\alpha(\tau) - \beta(\tau) dlnP/dlnk$, where α and β are functions related to linear growth funcion, and are calculated to be (0.6, 1.3) for $z = 1$ and (0.4, 0.9) for $z = 2$. [1] The 5 estimate them from density variance.

$$\begin{aligned}
\hat{\gamma}_1(\boldsymbol{x}) &= [\delta_g^{w_1}(\boldsymbol{x})\delta_g^{w_1}(\boldsymbol{x}) - \delta_g^{w_2}(\boldsymbol{x})\delta_g^{w_2}(\boldsymbol{x})], \\
\hat{\gamma}_2(\boldsymbol{x}) &= [2\delta_g^{w_1}(\boldsymbol{x})\delta_g^{w_2}(\boldsymbol{x})], \\
\hat{\gamma}_x(\boldsymbol{x}) &= [2\delta_g^{w_1}(\boldsymbol{x})\delta_g^{w_3}(\boldsymbol{x})], \qquad (11) \\
\hat{\gamma}_y(\boldsymbol{x}) &= [2\delta_g^{w_2}(\boldsymbol{x})\delta_g^{w_3}(\boldsymbol{x})], \\
\hat{\gamma}_z(\boldsymbol{x}) &= [(2\delta_g^{w_3}(\boldsymbol{x})\delta_g^{w_3}(\boldsymbol{x}) - \delta_g^{w_1}(\boldsymbol{x})\delta_g^{w_1}(\boldsymbol{x}) - \delta_g^{w_2}(\boldsymbol{x})\delta_g^{w_2}(\boldsymbol{x}))]/3,
\end{aligned}$$

(2) Reconstruct 3D density field.

$$\begin{aligned}
\kappa_{3\mathrm{D}}(\boldsymbol{k}) &= \frac{1}{k_1^2 + k_2^2 + k_3^2}[(k_1^2 - k_2^2)\gamma_1(\boldsymbol{k}) + 2k_1k_2\gamma_2(\boldsymbol{k}) \qquad (12) \\
&+ 2k_1k_3\gamma_x(\boldsymbol{k}) + 2k_2k_3\gamma_y(\boldsymbol{k}) + (2k_3^2 - k_1^2 - k_1^2)\gamma_z(\boldsymbol{k})].
\end{aligned}$$

Third, we correct bias and suppress noise with a Wiener filter. Due to the foregrounds, the noise in z direction will be different from x,y direction, therefore we apply an anisotropic Wiener filter.

$$\hat{\kappa}_c(\boldsymbol{k}) = \frac{\kappa_{3D}(\boldsymbol{k})}{b(k_\perp, k_\parallel)} W(k_\perp, k_\parallel)\ , \qquad (13)$$

Bias $b = \frac{P_{k3D\delta}}{P_\delta}$, Wiener filter $W = \frac{P_\delta}{P_{k3D}/b^2}$.

B. Cross Correlation Behavior with Tidal Reconstructed Field

1. Correlation of reconstructed velocity fields:

We first present the result about reconstructed velocity field(Eq.(1)) in Fig.1. The upper two panels show the cross correlation r between v_z and $\hat{v}_z^{fs}$ calculated from foreground substracted field δ_{fs}; the lower panel shows the cross correlation between v_z and $\hat{v}_z^{tide}$ calculated from $\hat{\kappa}_c$. The contour line represent the value of $k^3P(k)$, which is related to the importance of each mode when generating kSZ signals.

Notice: 1. Although the foreground at z=2 is stronger, the non-linear effects are weaker. Therefore, we can still see some correlations at $k\ \|\lesssim 0.1$, with the little density signals left. And these correlations are even better than the z=1 case after the gaussianization.

[1] The effect of the filter W_i on different scales could be seen in Appendix 1.

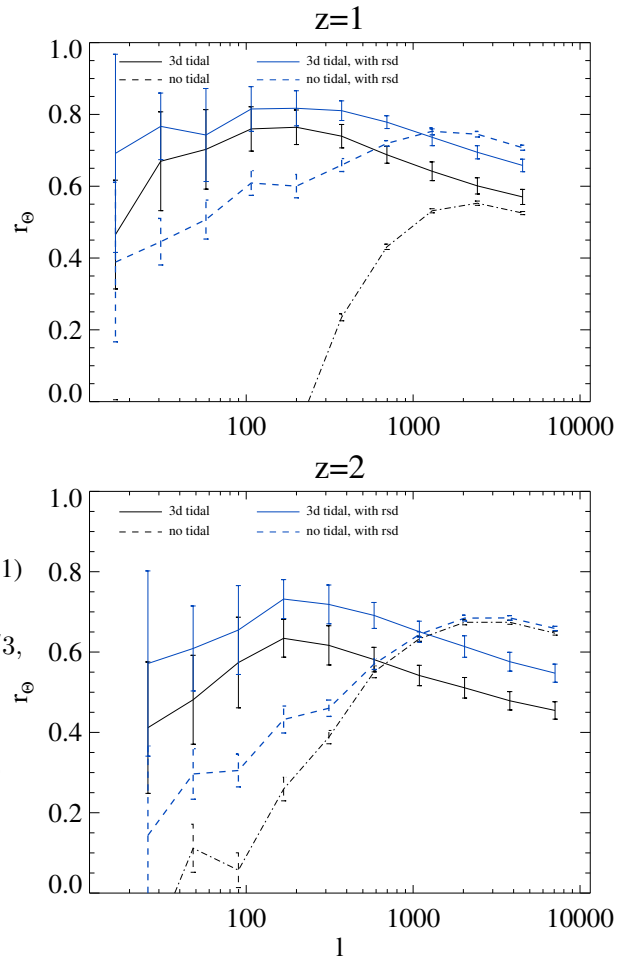

FIG. 2: The cross correlation r between reconstructed kSZ $P_{\hat{\Theta}_{kSZ}}$ and real kSZ $P_{\Theta_{kSZ}}$. (Dashed line) kSZ calculated from foreground substracted 21cm density field δ_{fs}; (Solid line) kSZ calculated from tidal reconstructed density field. (Blue lines) take into account of redshift distortions.

On the other hand, there is degrading performance of tidal reconstruction on z=2. This is likely due to the stricter cutoff $k_c = 0.32h/Mpc$ compared to $k_c = 0.5h/Mpc$ at z=1.

2. Since tidal reconstruction relies strongly on large k modes, and we only lost small k_z modes in the foreground(Fig.1 upper panel). The reconstruction on $k_\parallel$ is better than on $k_\perp$, which is an advantage for estimating v_z.

Important to see: 1. The previously lost small $k_\parallel$ modes has been well reconstructed through the 3D tidal reconstruction procedures. 2. The modes recovered in tidal reconstruction play more vital role in generating kSZ signals.

2. Correlation of reconstructed kSZ signals:

In Fig.2, we demonstrate the correlation r between the reconstructed kSZ signal $\hat{\Theta}$ and original kSZ signal Θ (black lines). We used both orginal foreground substracted density field and tidal reconstructed density field and compare the different results.

Important to see: 1. For z=1, there are significant improvement on the cross-correlation after tidal reconstruction, especially below $l \sim 2000$ 2. For z=2, the tidal reconstruction

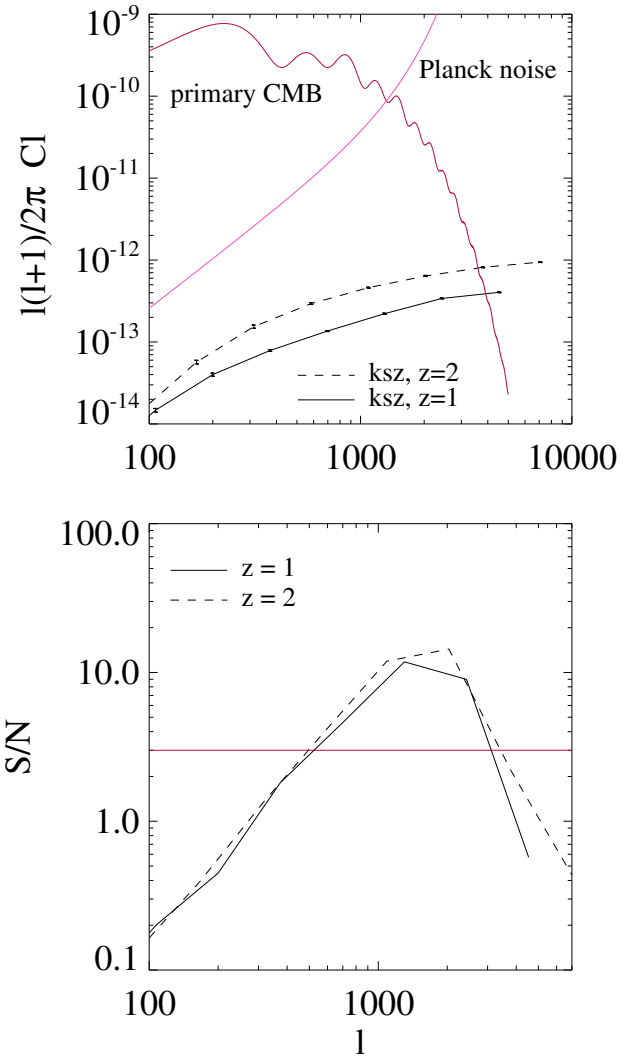

FIG. 3: (Top) Relative strength of kSZ signal, within a box of $\Delta\chi = 1200Mpc/h$. (Bottom) predicted S/N, assuming Planck noise, $\Delta l/l = 0.1$, $f_{sky} = 0.8$.

improves the cross-correlation for $l \lesssim 800$. However, since the non-linear effect is less strong at this stage, the orginal 21cm density field is good enough to reconstruct kSZ signal for $l \gtrsim 800$. Combining them, we would have good cross-correlation for $l \sim 20 - 8000$.

In all, for both redshift, with the non-ideal foregrounds and resolutions we assume, we are able to obtain a correlation $r \gtrsim 0.5$ for $l \sim 50 - 5000$ between 21cm density field and kSZ signals.

V. DISCUSSION AND ERROR ESTIMATES

A. Statistical Error

We use the statistical error to estimate the S/N ratio for real surveys. Taking into account the contamination from primary CMB and facility noises, it can be approximated as:

$$\frac{\Delta C_l}{C_l} \simeq \frac{1}{r\sqrt{(2l+1)\Delta l f_{sky}}}\sqrt{\frac{C_l^{\rm CMB} + C_l^{kSZ} + C_l^{\rm CMB,N}}{C_l^{kSZ,\Delta z}}} \quad (14)$$

Where C_l^{CMB} is the angular powerspectrum of primary CMB; $C_l^{CMB,N}$ indicates the facility noises; $C_l^{kSZ,\Delta z}$ is the kSZ signal from a certain redshift bin; r is the correlation coefficients we get; f_{sky} is the percent of sky area covered by both surveys.

In our case, we calculate C_l^{CMB} from CAMB [30]. We use Planck 2015 results [31] at 217GHz to estimate $C_l^{CMB,N}$. $C_l^{CMB,N} = (\sigma_{p,T}\theta_{FWHM})^2 W_l^{-2}$; where $\sigma_{p,T} = 8.7\mu K_{CMB}$ is Sensitivity per beam solid angle, $\theta_{FWHM} \sim 5'$ is the effective beam FWHM, $W_l = exp[-l(l+1)/2l_{beam}^2]$ is the smoothing window function, with $l_{beam} = \sqrt{8\ln 2}/\theta_{FWHM}$. We choose $f_{sky} = 0.8$, since it is feasible for 21cm intensity mapping to survey large sky areas. We choose $\Delta l/l = 0.1$. And for $C_l^{kSZ,\Delta z}$, we choose two bins of size 1200 Mpc/h, centered at redshift 1,2 respectively.

In Fig.3, we plot the S/N level for the two redshift bins. The S/N will exceeds 3 from $l \sim 500 - 3000$.

Since we only use the correlation calculated from tidal reconstructed field, the S/N shall be higher for z=2 combining tidal reconstructed field and foreground substracted field. Moreover, since C_l^{kSZ} is relatively flat, it is possible to bin it into larger Δl. eg. [18] choose $\Delta l = 200$, and this will yield better S/N for $l < 2000$ in Fig.3.

What's more, Planck's noise level is far from ideal. If we consider the case of 4th generation facilities, there will also be a giant leap for S/N at large l. However, in that case, we have to have accurate substraction for CMB lensing, when primary CMB dims out.

B. Redshift Distortion

We analyze the influence of linear redshift space distortion (RSD) in kSZ signal reconstruction. Equipped with it, we provide the very interesting results of adding RSD to simulations, and get better cross correlation (Fig.2). We also discuss another important advantage RSD brings.

The redshift distortions results from the radial peculiar velocity, which leads to a misjudgement of distance referring to Hubble flow.

In linear regions, it will induce an extra density contraction in redshift space:

$$\delta^{RSD}(\boldsymbol{k}) \approx (1 + f\frac{k_z^2}{k^2})\delta(\boldsymbol{k}) \quad (15)$$

where again $f = \frac{d\ln D}{d\ln a}$, with the cosmological parameter we choose, $f = 1.5, z \sim 1$; $f = 0.96, z \sim 2$.

Therefore, the easiest way to substract the linear RSD is to devide the δ^{RSD} we have by $1 + f\frac{k_z^2}{k^2}$ before all the calculations.

However, if we leave it here, since our foreground is in the same direction as the RSD, we will see some fortunate good effects. We discuss both the case of non-tidal reconstruction, and tidal reconstruction, and they are improved in different ways.

Note: in the following argument, small k refers to $k \sim 0.01h/Mpc$, larger k refers to $k > 0.1h/Mpc$, the powerspectrum of latter is around a magnitude smaller than the former.

(1) $\hat{\Theta}$ with RSD foreground substracted 21cm density field δ_{fs}^{RSD}.

Following Eq.(1), we can quickly write down the change for v(k):

$$\hat{v}_{z,fs}^{RSD}(\boldsymbol{k}) \propto \delta_{fs}^{RSD}(\boldsymbol{k})\frac{k_z}{k^2} \tag{16}$$

$$= \hat{v}_{z,fs}(\boldsymbol{k})(1 + f\frac{k_z^2}{k^2}) \tag{17}$$

The new term gives heavier weigh to modes with $k_\parallel \gg k_\perp$.

The real kSZ signal in Fourier space reads:

$$\Theta(\boldsymbol{k}_\perp) \equiv \Theta(k_x, k_y, 0) \propto \int d^3k \quad \delta(\boldsymbol{k}_\perp - \boldsymbol{k})v_z(\boldsymbol{k}) \tag{18}$$

$$\propto \int d^3k \;\; \delta(\boldsymbol{k}_\perp - \boldsymbol{k})\delta(\boldsymbol{k})\frac{k_z}{k^2}$$

For foreground substracted field the kSZ signal in Fourier space becomes:

$$\Theta_{fs}^{RSD}(\boldsymbol{k}_\perp) \propto \int d^3k \;\; \delta(\boldsymbol{k}_\perp - \boldsymbol{k})\delta_{fs}(\boldsymbol{k})\frac{k_z}{k^2}(1 + f\frac{k_z^2}{k^2}) \tag{19}$$

Notice, the first δ we use the original field, since this is the quantity we want to obtain in real cross correlating procedures.

seems to need a powerspectrum of P_δ

When $k_\perp$ is small:

In original kSZ signal, $\delta(\boldsymbol{k}_\perp - \boldsymbol{k}), \delta(\boldsymbol{k}), \frac{k_z}{k^2}$ reaches peak nearly at the same point when both $k_\perp, k_\parallel$ are small, and this dominates the signal. However, in the case of foreground substracted field, δ_{fs} is seriously reduced at small $k_\parallel$, and Θ_{fs} hense comes more from larger $k_\parallel$ which has little correlations with the original kSZ.

Fortunately, the RSD gives another term $1 + f\frac{k_z^2}{k^2}$, which give additional weigh to smaller $k_\parallel$ and partly compensate the weigh loss in foreground substraction. Therefore, we could have slightly better correlations in small $k_\perp$.

When $k_\perp$ is large:

$\delta(\boldsymbol{k}_\perp - \boldsymbol{k})$ and $\delta(\boldsymbol{k})$ no longer reach the peak simultaneously, and Θ comes from sum of a series of $k\prime$ from small to larger, hense the foreground substraction does not matter as much as in the case of $k_\parallel$, so both RSD and non-RSD case will have cross correlation.

(2) RSD influence to tidal reconstruction

After adding linear RSD, Eq.(11), each term will have two new weigh in Fourier space.

For simplicity, we define a demonstrator $\hat{\gamma}_{i,j}^{RSD}(\boldsymbol{x}) \equiv \delta_{RSD}^{w_i}(\boldsymbol{x})\delta_{RSD}^{w_j}(\boldsymbol{x})$.

In Fourier space, it becomes:

$$\hat{\gamma}_{RSD}(\boldsymbol{k}) = \int \frac{d^3k\prime}{(2\pi)^3}\delta^{w_i}(\boldsymbol{k} - \boldsymbol{k\prime})\delta^{w_j}(\boldsymbol{k\prime}) \tag{20a}$$

$$(1 + f\frac{(\boldsymbol{k} - \boldsymbol{k\prime})_z^2}{(\boldsymbol{k} - \boldsymbol{k\prime})^2})(1 + f\frac{k\prime_z^2}{k\prime^2})$$

$$= \int \frac{d^3k\prime}{(2\pi)^3}\delta_{fs}(\boldsymbol{k} - \boldsymbol{k\prime})S(|\boldsymbol{k} - \boldsymbol{k\prime}|)\delta_{fs}(\boldsymbol{k\prime})S(k\prime) \tag{20b}$$

$$\frac{(\boldsymbol{k} - \boldsymbol{k\prime})_i}{|\boldsymbol{k} - \boldsymbol{k\prime}|}\frac{k\prime_j}{k\prime}(1 + f\frac{(\boldsymbol{k} - \boldsymbol{k\prime})_z^2}{(\boldsymbol{k} - \boldsymbol{k\prime})^2})(1 + f\frac{k\prime_z^2}{k\prime^2})$$

From (20a) we can see that the shear estimators now favor information from $\delta(k)$ with $k\_parallel \gg k_\perp$ more than before.

From (20b) we see the influence on different gamma varies. The amplification will be maximized when the shape of the two new weigh $(1 + f\frac{k_z}{k^2}$ at most approches other terms, i.e. when $i = j = z$. Therefore $\hat{\gamma}_z$ will be influenced most, followed by $\hat{\gamma}_x, \hat{\gamma}_y$

In all, the RSD effect is a natual filter that weighs more the information on z direction, and down-weigh the information of large $k_\perp$ to small $k_\perp$.

Therefore, if we use 2D tidal reconstruction, RSD will cause a noticeable degration on the reconstruction (If we have RSD yet not have foreground, apply 3D tidal reconstruction, RSD may cause slight degration with However, fortunately, we have foreground which happen to be in the same direction with RSD. For z directions, only small $k_\parallel$ modes are lost, which do not matter much in the reconstruction; while for other directions sufficient amount of modes with $k_\perp$ from small to large are lost, and this leads to more inaccurate reconstruction on $k_\perp$ direction. And RSD serve as a natural filter to deal with that. 1

VI. CONCLUSION

VII. ACKNOWLEDGE

We acknowledge discussions with Kendrick Smith, Matthew Johnson, Wenkai Hu, Tianxiang Mao and Jiawei Shao. The simulations were performed on the BGQ supercomputer at the SciNet HPC Consortium. SciNet is funded by: the Canada Foundation for Innovation under the auspices of Compute Canada; the Government of Ontario; the Ontario Research Fund – Research Excellence; and the University of Toronto. Research at the Perimeter Institute is supported by the Government of Canada through Industry Canada and by the Province of Ontario through the Ministry of Research & Innovation. The Dunlap Institute is funded through an endowment established by the David Dunlap family and the University of Toronto.

[1] R. J. Cooke, M. Pettini, R. A. Jorgenson, M. T. Murphy, and C. C. Steidel, ApJ **781**, 31 (2014), 1308.3240.

[2] G. Hinshaw, D. Larson, E. Komatsu, D. N. Spergel, C. L. Bennett, J. Dunkley, M. R. Nolta, M. Halpern, R. S. Hill, N. Odegard, et al., ApJS **208**, 19 (2013), 1212.5226.

[3] E. Komatsu, K. M. Smith, J. Dunkley, C. L. Bennett, B. Gold, G. Hinshaw, N. Jarosik, D. Larson, M. R. Nolta, L. Page, et al., ApJS **192**, 18 (2011), 1001.4538.

[4] G. Hinshaw, D. Larson, E. Komatsu, D. N. Spergel, C. L. Bennett, J. Dunkley, M. R. Nolta, M. Halpern, R. S. Hill, N. Odegard, et al., ApJS **208**, 19 (2013), 1212.5226.

[5] U.-L. Pen, ApJ **510**, L1 (1999), astro-ph/9811045.

[6] A. M. Sołtan, A&A **460**, 59 (2006), astro-ph/0604465.

[7] M. Fukugita and P. J. E. Peebles, ApJ **616**, 643 (2004), astro-ph/0406095.

[8] J. K. Werk, J. X. Prochaska, J. Tumlinson, M. S. Peeples, T. M. Tripp, A. J. Fox, N. Lehner, C. Thom, J. M. O'Meara, A. B. Ford, et al., ApJ **792**, 8 (2014), 1403.0947.

[9] R. Davé, B. D. Oppenheimer, N. Katz, J. A. Kollmeier, and D. H. Weinberg, MNRAS **408**, 2051 (2010), 1005.2421.

[10] R. A. Sunyaev and Y. B. Zeldovich, Comments on Astrophysics and Space Physics **4**, 173 (1972).

[11] R. A. Sunyaev and I. B. Zeldovich, MNRAS **190**, 413 (1980).

[12] P. Zhang, U.-L. Pen, and H. Trac, MNRAS **347**, 1224 (2004), astro-ph/0304534.

[13] M. McQuinn, S. R. Furlanetto, L. Hernquist, O. Zahn, and M. Zaldarriaga, ApJ **630**, 643 (2005), astro-ph/0504189.

[14] O. Zahn, C. L. Reichardt, L. Shaw, A. Lidz, K. A. Aird, B. A. Benson, L. E. Bleem, J. E. Carlstrom, C. L. Chang, H. M. Cho, et al., ApJ **756**, 65 (2012), 1111.6386.

[15] N. Hand, G. E. Addison, E. Aubourg, N. Battaglia, E. S. Battistelli, D. Bizyaev, J. R. Bond, H. Brewington, J. Brinkmann, B. R. Brown, et al., Physical Review Letters **109**, 041101 (2012), 1203.4219.

[16] J. Shao, P. Zhang, W. Lin, Y. Jing, and J. Pan, MNRAS **413**, 628 (2011), 1004.1301.

[17] M. Li, R. E. Angulo, S. D. M. White, and J. Jasche, MNRAS **443**, 2311 (2014), 1404.0007.

[18] J. C. Hill, S. Ferraro, N. Battaglia, J. Liu, and D. N. Spergel, ArXiv e-prints (2016), 1603.01608.

[19] K. Bandura, G. E. Addison, M. Amiri, J. R. Bond, D. Campbell-Wilson, L. Connor, J.-F. Cliche, G. Davis, M. Deng, N. Denman, et al., in *Society of Photo-Optical Instrumentation Engineers (SPIE) Conference Series* (2014), vol. 9145 of *Society of Photo-Optical Instrumentation Engineers (SPIE) Conference Series*, p. 22, 1406.2288.

[20] Y. Xu, X. Wang, and X. Chen, ApJ **798**, 40 (2015), 1410.7794.

[21] http://www.acru.ukzn.ac.za/ hirax/.

[22] T. Di Matteo, B. Ciardi, and F. Miniati, MNRAS **355**, 1053 (2004), astro-ph/0402322.

[23] K. W. Masui, E. R. Switzer, N. Banavar, K. Bandura, C. Blake, L.-M. Calin, T.-C. Chang, X. Chen, Y.-C. Li, Y.-W. Liao, et al., ApJ **763**, L20 (2013), 1208.0331.

[24] E. R. Switzer, T.-C. Chang, K. W. Masui, U.-L. Pen, and T. C. Voytek, ApJ **815**, 51 (2015), 1504.07527.

[25] U.-L. Pen, R. Sheth, J. Harnois-Deraps, X. Chen, and Z. Li, ArXiv e-prints (2012), 1202.5804.

[26] H.-M. Zhu, U.-L. Pen, Y. Yu, X. Er, and X. Chen, ArXiv e-prints (2015), 1511.04680.

[27] J. Harnois-Déraps, U.-L. Pen, I. T. Iliev, H. Merz, J. D. Emberson, and V. Desjacques, MNRAS **436**, 540 (2013), 1208.5098.

[28] L. B. Newburgh, G. E. Addison, M. Amiri, K. Bandura, J. R. Bond, L. Connor, J.-F. Cliche, G. Davis, M. Deng, N. Denman, et al., in *Society of Photo-Optical Instrumentation Engineers (SPIE) Conference Series* (2014), vol. 9145 of *Society of Photo-Optical Instrumentation Engineers (SPIE) Conference Series*, p. 91454V, 1406.2267.

[29] X. Chen, International Journal of Modern Physics Conference Series **12**, 256 (2012), 1212.6278.

[30] A. Lewis, A. Challinor, and A. Lasenby, Astrophys. J. **538**, 473 (2000), astro-ph/9911177.

[31] Planck Collaboration, R. Adam, P. A. R. Ade, N. Aghanim, M. Arnaud, M. Ashdown, J. Aumont, C. Baccigalupi, A. J. Banday, R. B. Barreiro, et al., ArXiv e-prints (2015), 1502.01587.